Hybrid Continuous Wavelet Transform and GoogLeNet Framework for Accurate Classification of Power Quality Disturbances

Duy Anh Bui[1], *Bon Nhan Nguyen*[1], *Partha Kayal* [2,*]

[1]Faculty of Electrical and Electronics Engineering, Ho Chi Minh City University of Technology and Engineering, Ho Chi Minh City, Vietnam
[2]Department of Electrical Engineering, National Institute of Technology Silchar, Assam-788010, India

Corresponding Author: [2,]Partha Kayal (Email: partha@ee.nits.ac.in)
Co-Authors: [1]Duy Anh Bui (Email: 2430602@student.hcmute.edu.vn), [2]Bon Nhan Nguyen (Email: bonnn@hcmute.edu.vn)
(Received: 18-February-2026; accepted: 02-April-2026; published: 30-June-2026)
http://dx.doi.org/10.55579/jaec.2026102.539

Abstract. *Accurate classification of power quality disturbances (PQDs) is critical for maintaining grid stability amidst the increasing integration of renewable energy sources. However, traditional feature extraction methods and standard Convolutional Neural Networks (CNNs) struggle with non-stationary signals due to fixed-size convolutional kernels that cannot simultaneously capture features at multiple temporal and spectral scales. To address this limitation, this paper proposes a hybrid framework integrating Continuous Wavelet Transform (CWT) with the GoogLeNet (Inception v1) architecture. The method converts one-dimensional voltage waveforms into two-dimensional time-frequency scalograms, which are then processed by GoogLeNet's Inception modules—featuring parallel* 1×1, 3×3, *and* 5×5 *convolutional pathways—to extract multi-scale features simultaneously. Extensive experimental validation on a balanced dataset of 2,100 simulated samples across seven disturbance types demonstrates robust performance, achieving a mean classification accuracy of* $90.95\% \pm 1.60\%$ *over 10 independent trials, with best-case performance at* 93.29%. *Notably, frequency-domain disturbances (Harmonics and Oscillatory Transients) attain perfect classification (*100%, $\sigma = 0\%$*) across all trials. These results demonstrate that the proposed CWT–GoogLeNet framework effectively addresses the multi-scale feature extraction challenge, demonstrating reliable statistical performance for automated power quality monitoring in modern smart grid applications.*

Keywords: *power quality, disturbance classification, Wavelet transform, convolutional neural network (CNN).*

1. Introduction

Maintaining high power quality (PQ) is essential for the stable and reliable operation of modern electrical power systems, particularly in the context of increasing penetration of non-linear loads and renewable energy sources [1,2]. These integrations frequently introduce various power quality disturbances (PQDs), including voltage

sags, voltage swells, harmonics, and transient events. If such disturbances are not promptly detected and accurately classified, they may result in equipment overheating, data corruption, malfunction of sensitive loads, and significant economic losses [3, 4]. Consequently, the development of reliable and automated PQD classification systems has become a critical requirement for effective power system monitoring and protection.

Traditional PQD identification approaches mainly rely on handcrafted feature extraction techniques, such as the Fourier Transform, Short-Time Fourier Transform, or S-Transform, followed by shallow classifiers including Support Vector Machines (SVMs) and Decision Trees [5, 6]. Although these methods can yield satisfactory results for stationary or mildly non-stationary signals, they generally suffer from limited adaptability to complex time-varying disturbances. Moreover, their performance heavily depends on expert knowledge for feature engineering, parameter selection, and threshold tuning, which constrains their scalability and robustness in real-world applications. In recent years, deep learning models have emerged as effective alternatives by enabling automatic feature learning directly from raw data. Specifically, [7] proposed a closed-loop 1-D CNN architecture with batch normalization to automate feature extraction, thereby overcoming the limitations of manual methods. To address real-time constraints, [8] implemented a Deep Belief Network (DBN) on an embedded parallel computing platform, achieving high accuracy with low latency. In addition, [9] highlighted the complex harmonic challenges associated with offshore wind integration, underscoring the critical need for advanced classification systems in modern power grids.

Despite their success, conventional CNN architectures exhibit an inherent limitation in that they typically employ fixed-size convolutional kernels throughout the network [7]. This structural rigidity restricts their ability to simultaneously capture multi-scale characteristics of PQDs, such as long-duration, low-frequency voltage sags and short-duration, high-frequency oscillatory transients [10]. To overcome this limitation, recent studies have explored advanced architectures, including Transformer-based models [11, 12] and hybrid frameworks incorporating sophisticated time-frequency techniques such as the Wavelet Synchrosqueezed Transform (WSST) [13, 14]. However, these approaches often incur substantial computational complexity, which limits their feasibility for real-time or resource-constrained monitoring systems. Alternatively, lightweight networks such as MobileNet [15] and hybrid models combining deep feature extractors with classical classifiers (e.g., ResNet–SVM) [16] have been proposed to improve efficiency, yet they frequently involve trade-offs between model depth, representational capacity, and classification accuracy. Therefore, there remains a clear need for a streamlined framework that achieves an effective balance between multi-scale feature extraction capability and computational efficiency [17].

To address these challenges, this study proposes a hybrid classification framework that integrates the Continuous Wavelet Transform (CWT) with the GoogLeNet (Inception v1) architecture [18, 19]. In the proposed approach, one-dimensional voltage signals are first transformed into two-dimensional scalogram representations using CWT, thereby exposing their latent time–frequency characteristics. Unlike the Short-Time Fourier Transform (STFT), which suffers from fixed-resolution windows, CWT provides a high-resolution time–frequency representation that is particularly well-suited for analyzing non-stationary PQDs. These scalograms are subsequently fed into a GoogLeNet-based classifier. Furthermore, GoogLeNet is selected over more recent architectures such as Vision Transformers (ViTs) and EfficientNet based on both architectural characteristics and dataset constraints. Vision Transformers, while powerful, typically require large-scale datasets due to their lack of strong inductive biases, making them prone to overfitting on smaller, controlled datasets such as the 2,100-sample dataset used in this study. In contrast, GoogLeNet offers a balanced depth that enables stable training under limited data conditions. Compared to EfficientNet, which primarily relies on sequential convolutional scaling, the selection of GoogLeNet is motivated by its Inception modules, which employ parallel convolutional filters

with different kernel sizes (1×1, 3×3, 5×5) within a single block [19]. This architectural design is well aligned with the multi-resolution characteristics of CWT scalograms, enabling the network to analyze input features at multiple spatial resolutions simultaneously, allowing it to effectively capture both global spectral patterns and localized transient phenomena.

The main contributions of this paper are summarized as follows:

- An end-to-end hybrid classification framework is proposed by integrating CWT-based scalogram representations with a fine-tuned GoogLeNet architecture, effectively combining high-resolution time–frequency analysis with multi-scale feature extraction capabilities.
- The proposed architecture significantly outperforms conventional fixed-kernel CNN models in distinguishing morphologically similar PQDs, such as voltage sags and interruptions, as well as complex spectral distortions, including harmonics and transient events.
- The effectiveness and robustness of the proposed framework are validated on a rigorously simulated dataset comprising seven distinct PQD types, achieving an overall classification accuracy exceeding 93%, demonstrating its suitability for practical power quality monitoring applications.

2. Method

2.1. Method Overview

The proposed method in this study is illustrated through a general block diagram, as shown in Figure 1. The input of the system is a time-domain voltage signal, which is used to analyze and identify various power quality disturbance patterns. The input signal is first transformed into the time–frequency domain using the CWT, thereby generating scalogram images that represent the energy distribution of the signal over time and frequency. These scalogram images are then fed into a deep convolutional neural network based on the GoogLeNet architecture for feature extraction and classification. The output of the system corresponds to a label associated with one of seven power quality conditions, including normal, voltage sag, voltage swell, interruption, harmonic distortion, flicker, and transient disturbances.

To ensure accurate feature representation, the specific parameters for signal generation and CWT extraction are carefully configured. The input signals are generated with a fundamental frequency of 50 Hz, a sampling frequency of 10 kHz, and a signal window of 0.5 s. The CWT utilizes the Analytic Morse mother wavelet with 32 voices per octave to generate high-resolution time–frequency scalograms. Subsequently, these scalograms are mapped using a Jet colormap and resized to $224 \times 224 \times 3$ pixels to strictly match the 3-channel input layer requirements of the pre-trained GoogLeNet architecture.

2.2. Power Quality Disturbance Simulation

A sufficiently large and accurate dataset is crucial for the effective training of deep learning models. In this paper, following the comprehensive guidelines for PQD analysis detailed in [20], specific mathematical models are utilized to simulate six types of power quality disturbances, namely voltage sag, voltage swell, voltage interruption, harmonic distortion, voltage flicker, and transient oscillations, together with the standard sinusoidal waveform.

The baseline for our simulation is the normal voltage signal, representing an ideal steady-state condition maintained without any spectral contamination or amplitude deviation. This waveform is mathematically defined as [10]:

$$h(t) = A \sin(\omega t) \tag{1}$$

where $h(t)$ denotes the instantaneous voltage value at any given time instance t. The parameter A represents the nominal peak amplitude normalized to 1.0 per-unit (p.u.), and ω is the fundamental angular frequency corresponding to a system frequency f of 50 Hz.

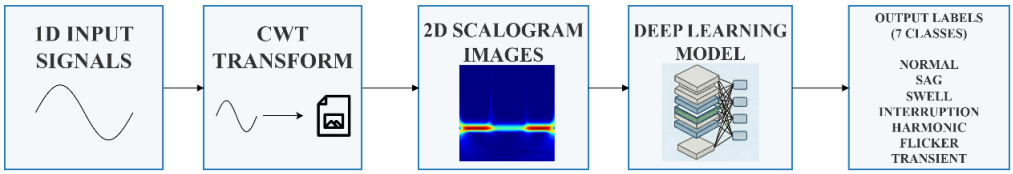

Figure 1: Overview of the proposed method.

A voltage sag represents a short-duration reduction in RMS voltage, typically caused by system faults or the startup of large motors, modeled as [10]:

$$h(t) = A\sin(\omega t)\left[1 - \alpha(-u(t-t_2) + u(t-t_1))\right] \tag{2}$$

where the parameter α determines the severity of the voltage drop, varying between 0.1 and 0.9 to simulate different fault impedances. The duration of the event is rigorously defined by the interval $[t_1, t_2]$ through the unit step functions $u(t)$.

In contrast to sags, a voltage swell is characterized by a temporary increase in the RMS voltage magnitude, often resulting from the de-energization of large loads or capacitor bank switching. This phenomenon is mathematically expressed as [10]:

$$h(t) = A\sin(\omega t)\left[1 + \alpha(-u(t-t_2) + u(t-t_1))\right] \tag{3}$$

This model shares a similar structure to Equation (2), but the coefficient α is added to the nominal amplitude to simulate a voltage rise. Here, α is restricted to the range of 0.1 to 0.8.

A voltage interruption is defined as the near-total loss of supply voltage, typically lasting from a few milliseconds to several seconds. While it utilizes the same mathematical structure as the voltage sag [10]:

$$h(t) = A\sin(\omega t)\left[1 - \gamma(-u(t-t_2) + u(t-t_1))\right] \tag{4}$$

The distinguishing feature here is the severity parameter γ. For an interruption simulation, γ is set strictly between 0.9 and 1.0, effectively reducing the signal amplitude to near zero during the fault interval.

Voltage flicker manifests as a continuous oscillation of the voltage envelope, often induced by arc furnaces or welding equipment, which leads to perceived unsteadiness in visual lighting. This disturbance is modeled as a low-frequency amplitude modulation of the fundamental carrier [21]:

$$h(t) = A\sin(\omega t)\left[1 + \alpha_f \sin(\beta\omega t)\right] \tag{5}$$

In Equation (5), two specific parameters define the envelope characteristics: α_f denotes the flicker intensity, typically set between 0.1 and 0.2, while β represents the modulation frequency fraction, simulating periodic fluctuations in the range of 5 Hz to 20 Hz.

Harmonic distortion arises from the operation of non-linear loads, such as power converters, which cause permanent deformation to the voltage waveform. This steady-state is modeled by superimposing specific odd-order frequency components onto the fundamental signal [21]:

$$\begin{aligned} h(t) = A\Big[&\alpha_3 \sin(3\omega t) + \alpha_5 \sin(5\omega t) \\ &+ \alpha_7 \sin(7\omega t) \\ &+ \alpha_1 \sin(\omega t)\Big] \end{aligned} \tag{6}$$

where the coefficients α_1, α_3, α_5, and α_7 determine the relative spectral weights of the fundamental, 3rd, 5th, and 7th harmonic orders, respectively. To ensure dataset diversity, these harmonic magnitudes are randomized within the range of 0.05 to 0.15.

Oscillatory transients are characterized by a sudden, high-frequency energy burst that decays exponentially over time. This phenomenon is modeled by injecting a damped sinusoidal wave

into the fundamental signal structure [21]:

$$h(t) = A\Big[\sin(\omega t) + \alpha(-u(t-t_2) + u(t-t_1)) \times \exp\left(-\frac{t-t_1}{\tau}\right) \times \sin(\omega_n(t-t_1))\Big] \tag{7}$$

In Equation (7), ω_n represents the natural frequency of the oscillation, typically ranging from 300 Hz to 900 Hz, while τ defines the time constant governing the signal's decay rate. Here, the coefficient α determines the initial peak intensity of the transient, while the time window $[t_1, t_2]$ strictly bounds the disturbance duration.

2.3. Continuous Wavelet Transform

The Wavelet Transform (WT) is a powerful tool for the analysis of transient phenomena, which was developed in the 1980s [22]. It provides effective feature extraction capability for fault diagnosis and prediction systems by enabling signal analysis across multiple frequency bands [23, 24]. Wavelet-based techniques are generally classified into two main forms: the Discrete Wavelet Transform (DWT) and the Continuous Wavelet Transform (CWT) [25]. In this paper, the CWT is employed because it allows signal features to be extracted over a wide range of frequency scales, thereby providing a more detailed time–frequency representation of the signal.

The continuous wavelet function is defined as follows [20]:

$$\omega_{s,\tau}(t) = \frac{1}{\sqrt{s}}\,\psi\left(\frac{t-\tau}{s}\right), \quad \text{with } s, \tau \in \mathbb{R} \text{ and } s \neq 0 \tag{8}$$

In this formulation, $\omega_{s,\tau}(t)$ represents the continuous wavelet family (daughter wavelets) derived from the mother wavelet $\psi(t)$, while $\mathbb{R}$ denotes the set of real numbers. The scale factor s dilates or compresses the function to capture low- or high-frequency features, respectively, while the translation parameter τ shifts the wavelet along the time axis to localize these features. The term $\frac{1}{\sqrt{s}}$ serves as a normalization factor, ensuring that the energy of the wavelet remains constant regardless of scale variation.

Physically, the CWT represents the localized time–frequency energy density of a non-stationary signal. By dynamically adjusting the scale factor s, the mother wavelet compresses to capture short-duration, high-frequency transients with high temporal resolution, and dilates to track long-duration, low-frequency variations like voltage sags with high spectral resolution. This multi-resolution capability allows the CWT to precisely isolate the exact time of occurrence and frequency boundaries of complex PQDs.

2.4. Deep Learning Network Based on GoogLeNet

This study employs GoogLeNet (Inception v1) as the feature extraction backbone for scalogram classification [19, 25]. The architecture's defining characteristic—parallel convolutional filters operating at multiple kernel sizes (1×1, 3×3, 5×5)—aligns well with the multi-scale nature of power quality disturbances, where events exhibit varying temporal durations and frequency bandwidths [1, 18]. The network's moderate depth of 22 layers provides sufficient representational capacity while maintaining training stability, a practical consideration given the limited availability of labeled PQ disturbance data compared to large-scale computer vision datasets [2, 7].

The model is initialized with ImageNet pretrained weights to leverage general visual feature representations [4]. To adapt the network for seven-class disturbance classification, the original 1000-way classifier is replaced with a custom architecture: a Dropout layer (rate = 0.4), a fully connected layer with 512 ReLU-activated neurons, a second Dropout layer (rate = 0.3), and a Softmax output layer. This configuration balances model capacity with regularization, preventing overfitting to the training set [26].

Training proceeds through a two-tier learning rate strategy. The pre-trained Inception modules undergo fine-tuning at a reduced learning rate of 1×10^{-4}, allowing gradual adaptation from natural image features to scalogram-specific patterns. Concurrently, the custom classifier trains from random initialization at 1×10^{-3}, enabling rapid convergence on task-specific decision boundaries. This differential learning approach retains the backbone's generalization ability while accelerating specialization to power quality classification [3].

3. Results and Simulation

In this section, the proposed CWT–GoogLeNet framework is evaluated to validate its effectiveness in classifying seven power quality disturbance types: Oscillatory Transient, Voltage Swell, Normal, Voltage Interruption, Voltage Flicker, Voltage Sag and Harmonic Distortion. A balanced dataset of 2,100 synthetic signals (300 samples per class) is generated according to IEEE 1159-2019 standards, with randomized parameters to ensure diversity. For instance, voltage sags vary between 0.1 and 0.9 p.u. with durations ranging from 0.05 to 0.30 seconds, while harmonic distortion incorporates 3rd, 5th, and 7th orders with total harmonic distortion (THD) levels between 8.7% and 26%. All signals are sampled at 10 kHz over a 0.5-second window (25 cycles at 50 Hz fundamental frequency).

The simulations are executed on a laptop with an AMD Ryzen 7 8845HS processor (3.80 GHz), 16 GB DDR5 RAM (5600 MT/s), and an NVIDIA GeForce RTX 3050 GPU (6 GB VRAM), running Windows 11 Home (64-bit). MATLAB R2023b is used for signal generation, wavelet preprocessing, and neural network training.

3.1. Simulation Data Generation Results

This subsection focuses on the simulation-based generation of power quality disturbance signals used in this study. Based on the disturbance models introduced in Section 2, representative voltage waveforms corresponding to seven power quality disturbance types are synthetically generated under controlled parameter settings. The simulation process is designed to ensure physical interpretability while maintaining sufficient variability within each disturbance class. These simulated signals constitute the input for subsequent time–frequency analysis and deep learning–based classification. Typical examples of the generated waveforms are illustrated in Figures 2–8.

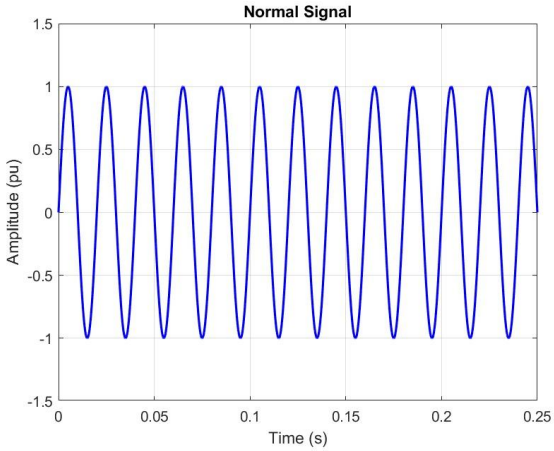

Figure 2: Examples of Normal signal waveform.

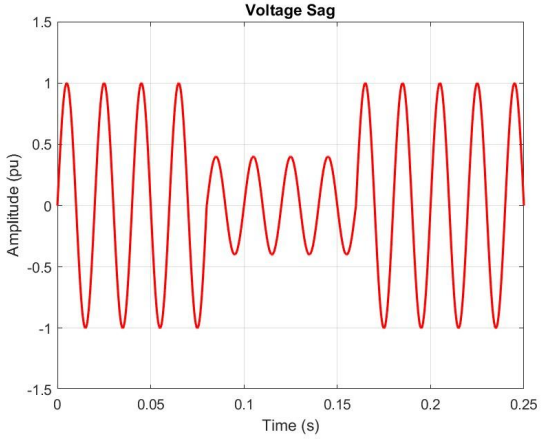

Figure 3: Examples of Voltage Sag waveform.

The simulated waveforms presented in Figures 2–8 illustrate the distinct temporal signatures of each PQD based on the mathematical models defined in Equations (1)–(7). While

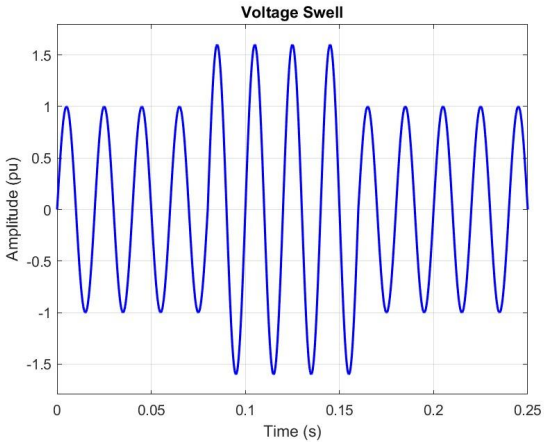

Figure 4: Examples of Voltage Swell waveform.

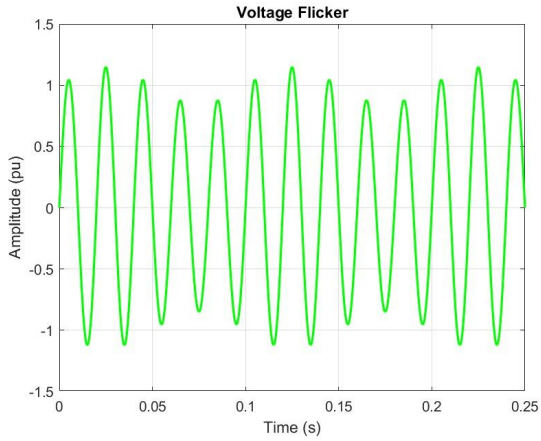

Figure 6: Examples of Voltage Flicker waveform.

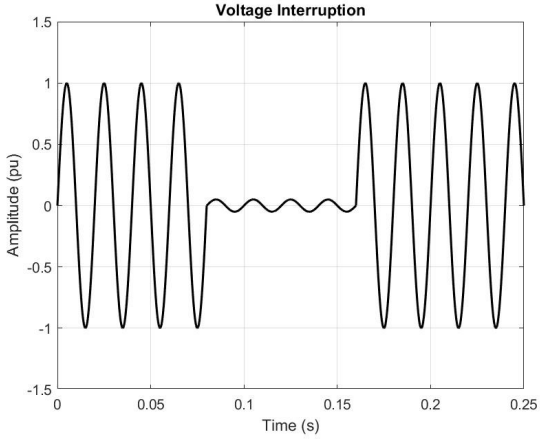

Figure 5: Examples of Voltage Interruption waveform.

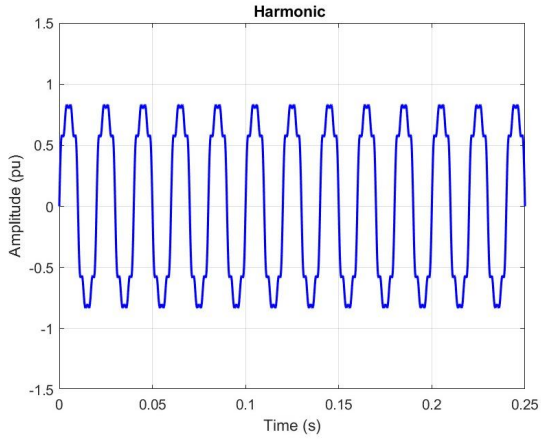

Figure 7: Examples of Harmonics waveform.

the normal signal shown in Figure 2 maintains a stable 50 Hz sinusoidal profile, the other categories exhibit specific deviations in amplitude, frequency, or waveform symmetry. Specifically, the voltage swell in Figure 4 displays clear amplitude-based variations with a distinct increase in peak magnitude. This behavior contrasts with the partial reduction of the sag observed in Figure 3 and the severe signal loss of the interruption depicted in Figure 5. These visual differences primarily affect the fundamental frequency component but remain structurally periodic.

Furthermore, complex distortions alter the waveform shape significantly. The voltage flicker in Figure 6 displays a low-frequency envelope, reflecting the amplitude modulation characteristic described in Equation (5). In contrast, the harmonic distortion in Figure 7 reveals a jagged, non-sinusoidal profile caused by the superposition of odd-order multiples. Finally, the oscillatory transient in Figure 8 represents the most abrupt change, featuring a high-frequency burst that rapidly decays. This localized energy concentration is a critical feature that visually distinguishes transients from the continuous, steady-state distortion observed in harmonics.

To validate the effectiveness of the proposed classification framework, a comprehensive synthetic dataset was generated based on the mathematical models presented in Section 2.2. . All

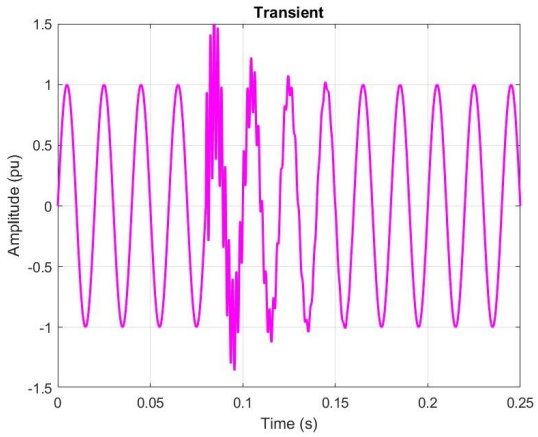

Figure 8: Examples of Transient waveform.

simulations were conducted in the MATLAB environment with a sampling frequency of $f_s = 10000$ Hz, corresponding to 64 samples per fundamental cycle at 50 Hz. This configuration ensures adequate temporal resolution for capturing both steady-state distortions and high-frequency transient phenomena. To enhance the generalization capability of the deep learning model and accurately emulate practical measurement environments, stochastic variations were systematically introduced during data generation. While the fundamental system frequency was fixed at 50 Hz, key disturbance parameters—including the fault initiation time (t_1), disturbance duration ($t_2 - t_1$), and amplitude-related coefficients (α)—were randomly sampled within their theoretical bounds. Furthermore, to simulate standard industrial sensor conditions, Additive White Gaussian Noise (AWGN) with a standard deviation of 0.01 p.u. (yielding an approximate Signal-to-Noise Ratio of 37 dB) was superimposed onto all generated waveforms. This strategy introduces significant intra-class variability and real-world robustness while preserving the intrinsic characteristics of each disturbance type.

Representative time-domain waveforms verifying the fidelity of these simulations are illustrated in Figures 2–8. The final dataset consists of 2,100 signal samples, evenly distributed across seven disturbance classes, with 300 samples per class. This balanced class distribution effectively mitigates the class imbalance issue and prevents bias toward dominant categories during training. The dataset was divided into training and testing subsets using an 80:20 ratio. Overall, the generated dataset provides a controlled yet sufficiently challenging benchmark for evaluating the robustness and generalization performance of the proposed CWT–GoogLeNet-based classification framework under diverse operating conditions.

3.2. Time–Frequency Feature Analysis

In this study, the Analytic Morse wavelet ($\gamma = 3, \beta = 60$) was employed to perform the CWT on voltage signals, generating scalograms with 128 logarithmically spaced frequency scales ranging from 1 Hz to 1 kHz. The Jet colormap was used to encode energy density, where warm colors (red/orange) indicate high wavelet coefficient magnitudes and cool colors (blue) represent background noise levels. This transformation converts one-dimensional temporal signals into two-dimensional time–frequency representations, revealing discriminative features that remain latent in the time domain alone.

Figure 9 establishes the baseline representation. The voltage sag in Figure 10 exhibits distinct energy attenuation during the fault interval $[t_1, t_2]$ (as mathematically modeled in Equation (2)), while the voltage swell in Figure 11 demonstrates an amplified response within the same frequency band. Furthermore, the voltage interruption presented in Figure 12 produces the most severe pattern, characterized by near-zero coefficients across all frequency scales that result in a distinct temporal gap. Spectral distortions manifest more complex time–frequency signatures. For instance, Figure 13 illustrates how voltage flicker introduces periodic envelope modulation at sub-25 Hz frequencies superimposed on the fundamental component. Similarly, the Harmonics signal scalogram in Figure 14 generates multiple parallel bands at 150, 250, 350 Hz, corresponding to the 3rd-, 5th-, and 7th-order harmonics introduced by nonlinear loads. Finally, the Transient signal depicted in Figure 15 produces a concentrated vertical energy burst extending up to 900 Hz, which decays exponentially within 10–50 ms, characteristic of capaci-

tor switching events. These results confirm that each disturbance class possesses a unique spectral fingerprint. The multi-resolution decomposition capability of the CWT enables simultaneous localization of transient spikes and sustained frequency components, thereby providing spatially structured input features that substantially enhance pattern recognition performance compared to raw waveform analysis. All resulting scalograms were resized to 224×224 pixels using bicubic interpolation and normalized to the range $[0, 1]$ prior to network training.

3.3. Classification Performance

1) Classification Performance

The GoogLeNet model was trained on the 2,100 scalogram samples, randomly partitioned into 1,680 training samples (80%) and 420 validation samples (20%). By initializing with ImageNet pre-trained weights, the network rapidly adapted to power quality feature representations without requiring prolonged training. Figure 16 depicts the training dynamics over 40 epochs, revealing stable convergence characteristics across both accuracy and loss metrics.

During the initial phase (Epochs 1–10), validation accuracy increased sharply from a random baseline ($\sim$ 14% for a seven-class chance level) to approximately 75%, while the training loss decreased significantly from 1.95 to 0.68. This rapid improvement demonstrates the effective transfer of low-level edge and texture features from natural images to scalogram patterns. In the fine-tuning phase (Epochs 10–30), the controlled learning rate decay (factor of 0.5 every 10 epochs) stabilized the optimization trajectory. Notably, the validation accuracy closely tracked the training accuracy throughout this interval, with a consistent gap of less than 2%, indicating that the dropout regularization (rates of 0.4 and 0.3) and weight decay ($\lambda_{wd} = 1 \times 10^{-4}$) successfully mitigated overfitting.

The model reached convergence in the final stage (Epochs 30–40), achieving a peak validation accuracy of 93.29% at Epoch 37 with a corresponding validation loss of 0.2527, as illustrated in Figure 16. Training accuracy stabilized at 94.81%, yielding a train–validation gap of just 1.74%, which remains well within acceptable bounds for generalization. The entire training process was completed in approximately 20 minutes using a batch size of 32, demonstrating sufficient efficiency for iterative model development. These results confirm the feasibility of the proposed approach for integration into real-time power quality monitoring systems, where periodic model retraining may be required to adapt to evolving grid conditions.

2) Overall Classification Accuracy and Confusion Matrix

To assess the model's classification performance beyond aggregate metrics, Figure 17 presents the confusion matrix evaluated on a held-out test set of 462 samples (66 per class, ensuring balanced evaluation). The model achieved an overall accuracy of 93.29%, with performance exhibiting a distinct dichotomy between frequency-dominant and amplitude-dominant disturbance types.

Consistent with the multi-resolution capabilities of the Continuous Wavelet Transform, the model demonstrated perfect classification for Harmonics and Oscillatory Transients (100% accuracy, 66/66 samples each). These classes possess invariant spectral signatures—parallel horizontal bands at harmonic frequencies and localized vertical bursts, respectively—that remain unaffected by amplitude normalization. The morphological distinctiveness of these patterns enables the Inception modules to extract highly discriminative features with minimal inter-class confusion. In contrast, classification errors were localized within amplitude-modulated categories: voltage swell, voltage interruption, and voltage sag. Most notably, the confusion matrix shows that 8 voltage swell and 7 voltage interruption samples were misclassified as voltage sag. This ambiguity represents an inherent, necessary trade-off in the proposed framework: while the Minimum–Maximum (Min–Max) normalization is strictly required to map the scalograms into the $[0, 1]$ range to leverage the pretrained weights of GoogLeNet, this technique effectively eliminates absolute amplitude distinc-

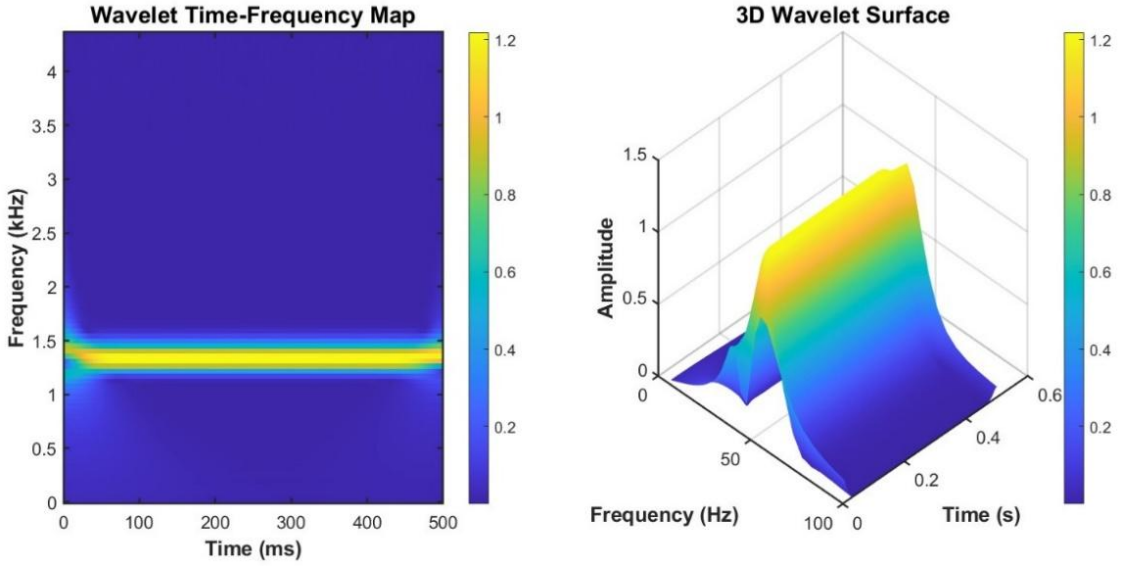

Figure 9: Scalogram and Wavelet-based spectrum of the voltage Normal signal.

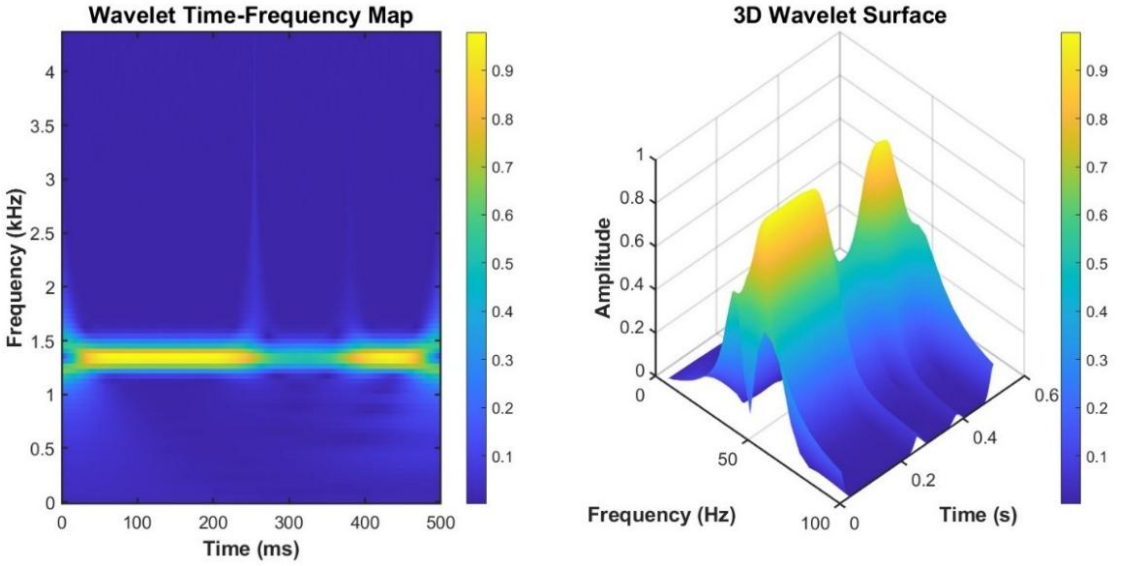

Figure 10: Scalogram and Wavelet-based spectrum of the voltage Sag signal.

tions. As a result, the network is forced to rely on the spatial energy distribution around the 50 Hz fundamental frequency, which renders the morphological signatures of voltage depressions and elevations nearly identical. Furthermore, the IEEE 1159 standard [27] defines voltage sags within the range of 0.1–0.9 p.u. and interruptions as values below 0.1 p.u., resulting in a narrow decision boundary of only 0.1 p.u. When combined with amplitude suppression during normalization, this tight margin inevitably leads to misclassification in borderline cases (e.g., voltage magnitude is within 0.08 and 0.12 p.u.).

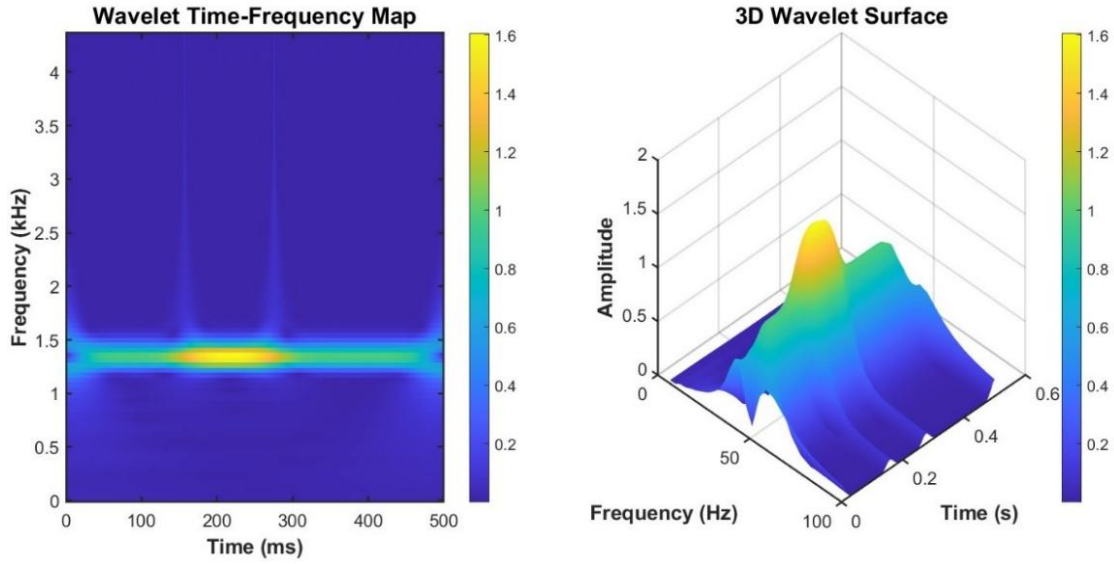

Figure 11: Scalogram and Wavelet-based spectrum of the voltage Swell signal.

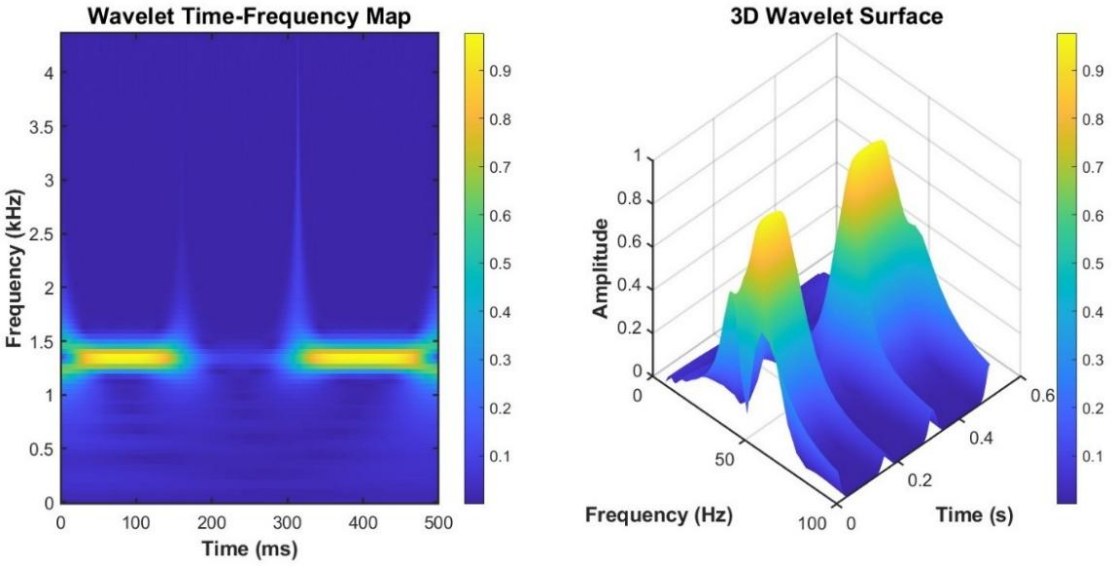

Figure 12: Scalogram and Wavelet-based spectrum of the voltage Interruption signal.

3) Statistical Stability and Reliability Analysis

While Section 3.3.2 highlighted the optimal performance capability of the proposed architecture, deep learning optimization is inherently stochastic in nature. To assess the reliability and reproducibility of the model under different random initialization conditions, a comprehensive statistical stability analysis was conducted through multiple independent experimental trials. The statistical results, summarized in Table 1, incorporate all 10 independent trials to fully reflect the model's operational performance variability. While computational resource constraints associated with training deep convo-

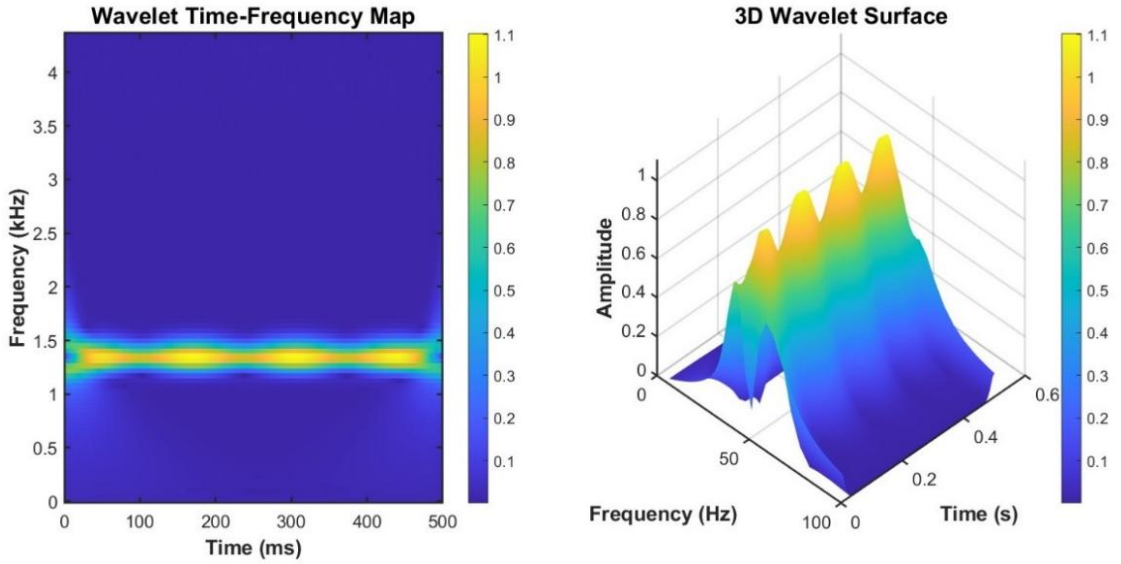

Figure 13: Scalogram and Wavelet-based spectrum of the voltage Flicker signal.

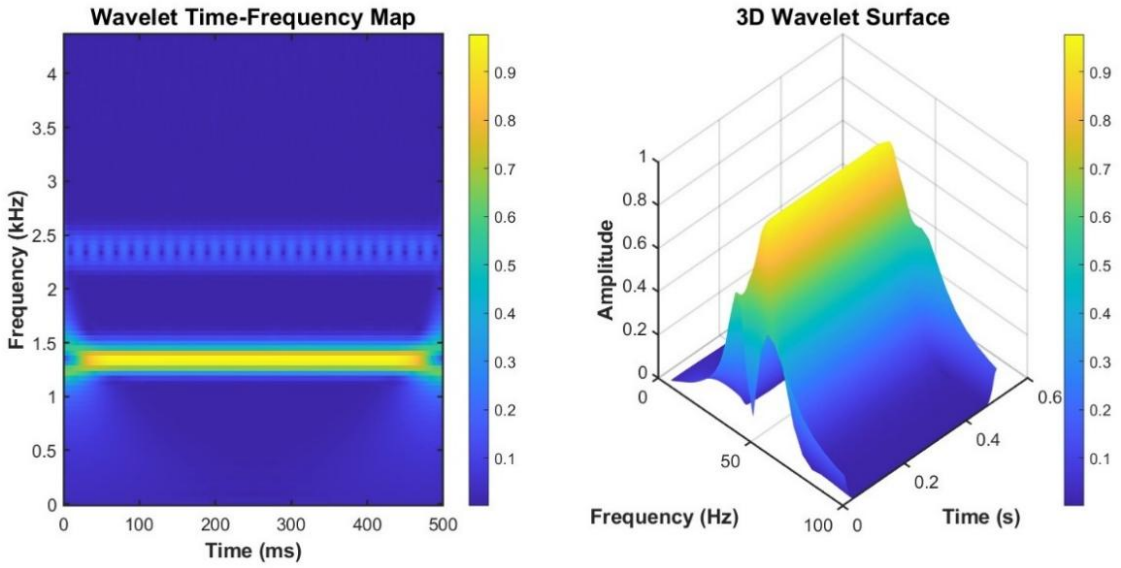

Figure 14: Scalogram and Wavelet-based spectrum of the Harmonics signal.

lutional networks limited the number of runs, these 10 trials serve as a robust preliminary indicator of the model's operational performance variability rather than an exhaustive statistical proof. The proposed system achieved a robust mean classification accuracy of 90.95%, accompanied by a low standard deviation of 1.60%. Across all trials, the classification accuracy ranged from a minimum of 88.31% to a maximum of 93.29%. This narrow performance dispersion demonstrates that the achieved accuracy is consistent and reproducible, rather than being attributable to a favorable or "lucky" initialization. A detailed comparison of the confusion matrices across trials reveals that performance variations are not uniformly distributed

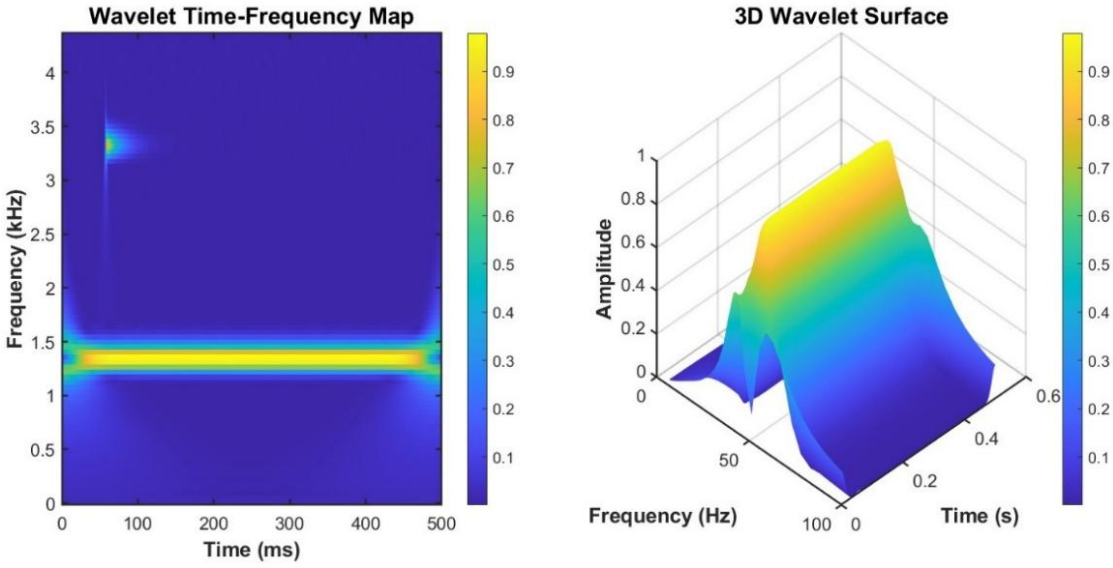

Figure 15: Scalogram and Wavelet-based spectrum of the Transient signal.

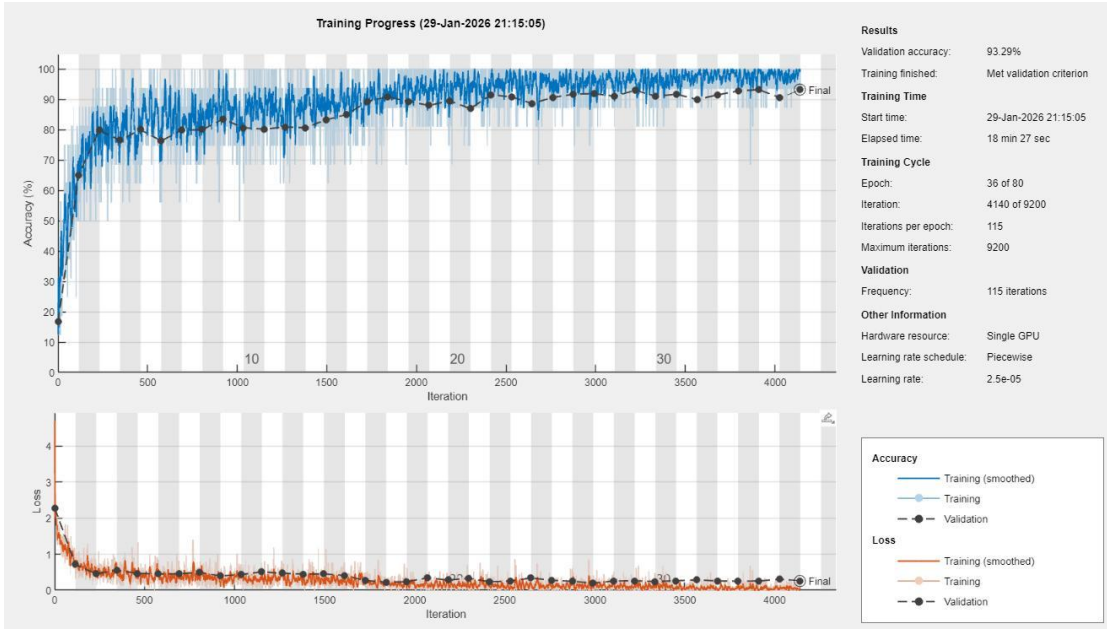

Figure 16: Training results of GoogLeNet.

among disturbance classes. Frequency-domain disturbances, including harmonics and transients, exhibited exceptional stability, consistently achieving near-perfect classification accuracy in all experimental runs. In contrast, fluctuations in overall accuracy were predominantly driven by ambiguity among amplitude-modulated disturbance classes. Specifically, in lower-performing trials (e.g., 88.31%), increased misclassification between Voltage Sag and Interruption was observed, whereas in higher-performing trials (e.g., 93.29%), this confusion was significantly reduced. These observations indicate that the proposed CWT–GoogLeNet

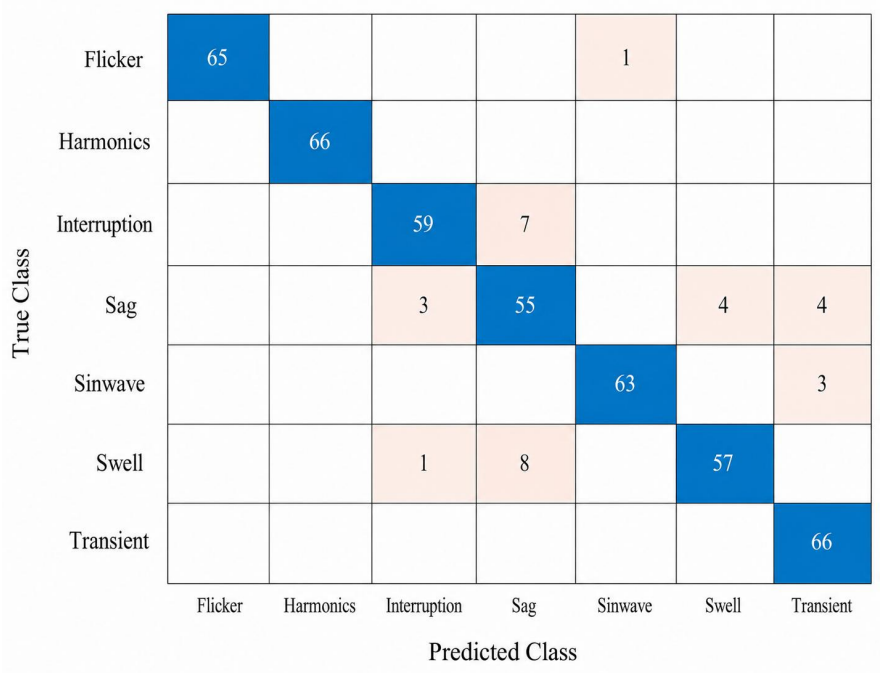

Figure 17: Confusion Matrix.

framework exhibits strong statistical robustness and reliability for practical power quality monitoring applications. Nevertheless, the discrimination of disturbance classes characterized by narrow amplitude margins remains the most sensitive aspect of the model, particularly with respect to random weight initialization during training.

Table 1: Statistical Performance over Independent Trials.

Metric	Value
Maximum Accuracy	93.29%
Minimum Accuracy	88.31%
Mean Accuracy (μ)	90.95%
Standard Deviation (σ)	1.60%

4. Conclusion

This study successfully established a robust automated framework for PQD classification by integrating the CWT with a fine-tuned GoogLeNet architecture. By converting one-dimensional voltage signals into two-dimensional time–frequency scalograms, the proposed method effectively overcomes the limitations of traditional manual feature extraction and standard CNNs that struggle with non-stationary signal characteristics. Experimental results on a dataset of seven distinct disturbance types demonstrate the efficacy of the proposed approach. The model achieved a peak classification accuracy of 93.29%, with an average accuracy of 90.95% and a standard deviation of 1.60% across multiple trials, indicating high statistical stability. Notably, the system attained 100% accuracy in identifying frequency-domain disturbances such as Harmonics and Oscillatory Transients. Compared to conventional fixed-kernel CNN architectures, the utilization of GoogLeNet's Inception modules proved to be a critical advantage. The parallel processing of multiple kernel sizes (1×1, 3×3, and 5×5) enabled the simultaneous capture of both long-duration voltage variations and high-frequency transient bursts. This multi-scale capability addresses the fundamental limitation of single-scale architectures, which cannot process fea-

tures at varying temporal and spectral resolutions within a single layer.

A targeted limitation was observed in differentiating Voltage Sags from Interruptions, attributed to Min–Max normalization suppressing absolute amplitude information. While this represents a necessary trade-off to leverage pre-trained network capabilities, this weakness is confined to amplitude-similar disturbance classes and does not affect the model's perfect classification performance for frequency-domain categories. Despite this limitation, the proposed framework maintains robust accuracy suitable for deployment in substation monitoring applications.

By enabling automated disturbance detection with minimal computational overhead, this framework addresses critical operational needs for utilities managing increasingly complex power grids with high renewable energy penetration. Future work will pursue four specific directions: (1) incorporating amplitude-preserving normalization techniques (e.g., z-score standardization) to resolve the Sag–Interruption ambiguity, (2) validating performance on IEC 61000-4-30 compliant field measurements from operational substations, (3) optimizing the network for edge deployment through model quantization, targeting inference latency below 15 ms on ARM-based processors, and (4) conducting exhaustive statistical validation over a larger number of independent trials and extended datasets to firmly establish the model's reliability bounds.

Acknowledgement

We thank Ho Chi Minh City University of Technology and Engineering for supporting this research.

References

[1] G. S. Chawda, A. G. Shaik, M. Shaik, S. Padmanaban, J. B. Holm-Nielsen, O. P. Mahela, and P. Kaliannan. Comprehensive review on detection and classification of power quality disturbances in utility grid with renewable energy penetration. *IEEE Access*, 8:146807-146830, 2020. DOI: 10.1109/ACCESS.2020.3014732

[2] M. A. Rodriguez-Guerrero, R. Carranza-Lopez-Padilla, R. A. Osornio-Rios, and R. D. J. Romero-Troncoso. A novel methodology for modeling waveforms for power quality disturbance analysis. *Electric power systems research*, 143:14-24, 2017. DOI: 10.1016/j.epsr.2016.09.003

[3] I. Topaloglu. Deep learning based a new approach for power quality disturbances classification in power transmission system. *Journal of Electrical Engineering & Technology*, 18(1):77-88, 2023. DOI: 10.1007/s42835-022-01177-1

[4] I. S. Samanta, S. Panda, P. K. Rout, M. Bajaj, M. Piecha, V. Blazek, and L. Prokop. A comprehensive review of deep-learning applications to power quality analysis. *Energies*, 16(11):4406, 2023. DOI: 10.3390/en16114406

[5] M. S. Priyadarshini, M. Bajaj, L. Prokop, and M. Berhanu. Perception of power quality disturbances using Fourier, Short-Time Fourier, continuous and discrete wavelet transforms. *scientific reports*, 14(1):3443, 2024. DOI: 10.1038/s41598-024-53792-9

[6] N. Minh Khoa and L. Van Dai. Detection and classification of power quality disturbances in power system using modified-combination between the stockwell transform and decision tree methods. *Energies*, 13(14):3623, 2020. DOI: 10.3390/en13143623

[7] S. Wang and H. Chen. A novel deep learning method for the classification of power quality disturbances using deep convolutional neural network. *Applied energy*, 235:1126-1140, 2019. DOI: 10.1016/j.apenergy.2018.09.160

[8] Z. Chen, M. Li, T. Ji, and Q. Wu. Real-time recognition of power quality disturbance-based deep belief network using embedded parallel computing platform.

IEEJ Transactions on Electrical and Electronic Engineering, 15(4):519–526, 2020. DOI: 10.1002/tee.23084

[9] H. Shao, R. Henriques, H. Morais, and E. Tedeschi. Power quality monitoring in electric grid integrating offshore wind energy: A review. *Renewable and Sustainable Energy Reviews*, 191:114094, 2024. DOI: 10.1016/j.rser.2023.114094

[10] K. Cai, W. Cao, L. Aarniovuori, H. Pang, Y. Lin, and G. Li. Classification of power quality disturbances using Wigner-Ville distribution and deep convolutional neural networks. *IEEE Access*, 7:119099–119109, 2019. DOI: 10.1109/ACCESS.2019.2937193

[11] U. Sipai, R. Jadeja, N. Kothari, T. Trivedi, and K. K. Ram. Deep transfer learning approach for the classification of single and multiple power quality disturbances. *Scientific Reports*, 15(1):34583, 2025. DOI: 10.1038/s41598-025-18064-0

[12] A. M. Saber, A. Selim, M. M. Hammad, A. Youssef, D. Kundur, and E. El-Saadany. A novel approach to classify power quality signals using vision transformers. In *Iecon 2024-50th annual conference of the IEEE industrial electronics society*, pp. 1–6. IEEE, 2024. DOI: 10.1109/IECON55916.2024.10905293

[13] I. S. Samanta, P. K. Rout, K. Swain, S. Mishra, and M. Cherukuri. Feature Extraction and Classification of Power Quality Disturbances Using Optimized Tunable-Q Wavelet Transform and Incremental Support Vector Machine. *International Transactions on Electrical Energy Systems*, 2024(1):1335666, 2024. DOI: 10.1155/2024/1335666

[14] J. Jiang, H. Wu, C. Zhong, and H. Song. Classification of power quality disturbances in microgrids using a multi-level global convolutional neural network and SDTransformer approach. *PloS one*, 20(2):e0317050, 2025. DOI: 10.1371/journal.pone.0317050

[15] P. M. Peruman and K. Ayyar. Power quality disturbance identification using hybrid deep learning in renewable energy systems. *Scientific Reports*, 15:44592, 2025. DOI: 10.1038/s41598-025-28291-0

[16] Z. Hou, B. Wang, J. Liu, Y. He, and Y. Yao, Physics-inspired time-frequency feature extraction and lightweight neural network for power quality disturbance classification, *Frontiers in Physics)*, 13:1616367, 2025. DOI: 10.3389/fphy.2025.1616367

[17] S. Akkaya. Optimization of Convolutional Neural Networks for Classifying Power Quality Disturbances Using Wavelet Synchrosqueezed Transform. *Traitement du Signal*, 41(2):599-614, 2024. DOI: 10.18280/ts.410205

[18] W. Hong, Z. Liu, and X. Wu. Power quality disturbance recognition based on wavelet transform and convolutional neural network. In *2021 IEEE international conference on artificial intelligence and computer applications (ICAICA)*, pp. 193–197, IEEE, 2021. DOI: 10.1109/TPWRD.2021.3095209

[19] C. Szegedy, W. Liu, Y. Jia, P. Sermanet, S. Reed, D. Anguelov, D. Erhan, V. Vanhoucke, and A. Rabinovich. Going deeper with convolutions. In *Proceedings of the IEEE conference on computer vision and pattern recognition*, pp. 1–9, 2015. DOI: 10.1109/CVPR.2015.7298594

[20] D. P. Mishra and P. Ray. Fault detection, location and classification of a transmission line. *Neural Computing and Applications*, 30(5):1377–1424, 2018. DOI: 10.1007/s00521-017-3295-y

[21] F. Jandan, S. Khokhar, Z. Memon, and S. Shah. Wavelet based simulation and analysis of single and multiple power quality disturbances. *Engineering, Technology & Applied Science Research*, 9(2):3909–3914, 2019. DOI: 10.48084/etasr.2409

[22] I. Daubechies, The wavelet transform, time-frequency localization and signal analysis, IEEE transactions on information theory, 36(5):961–1005, 1990. DOI: 10.1109/18.57199

[23] N. H. Phuc, T. Q. Khanh, and N. N. Bon, Discrete wavelet transform technique application in identification of power quality disturbances, VNUHCM Journal of Science and Technology Development, 9(1):47–56, 2006.

[24] S. Santoso, E. J. Powers, W. M. Grady, and P. Hofmann. Power quality assessment via wavelet transform analysis. *IEEE transactions on Power Delivery*, 11(2):924–930, 1996. DOI: 10.1109/61.489353

[25] N. N. Bon. Fault Identification, Classification, and Location on Transmission Lines Using Combined Machine Learning Methods. *International Journal of Engineering & Technology Innovation*, 12(2):91-109, 2022. DOI: 10.46604/ijeti.2022.7571

[26] W. Samek, G. Montavon, S. Lapuschkin, C. J. Anders, and K. R. Müller. Explaining deep neural networks and beyond: A review of methods and applications. *Proceedings of the IEEE*, 109(3):247–278, 2021. DOI: 10.1109/JPROC.2021.3060483

[27] IEEE. IEEE Recommended Practice for Monitoring Electric Power Quality, IEEE Standard 1159-2019 (Revision of IEEE Std 1159-2009). *IEEE Std*, pp. 1159–2019, 2019. DOI: 10.1109/IEEESTD.2019.8796486

About Authors

Duy Anh Bui received the M.S. degree in Electrical Engineering from Ho Chi Minh City University of Technology and Education (HCMUTE), Vietnam, in 2026. His research interests include power quality disturbances, advanced signal processing using wavelet techniques, and the application of deep learning architectures, such as CNNs and Transformers, in smart grid monitoring. He can be contacted at email: 2430602@student.hcmute.edu.vn.

Bon Nhan Nguyen received the Ph.D. degree in Electrical Engineering. He is currently a Senior Lecturer with the Faculty of Electrical and Electronic Engineering, Ho Chi Minh City University of Technology and Education (HCMUTE), Vietnam. His research focuses on power quality analysis, harmonic mitigation, and the application of artificial intelligence in power system fault identification. His expertise also extends to electromagnetic transient modeling, optimization in smart grids with distributed energy resources, and the enhancement of engineering education methodologies. He can be reached via email: bonnn@hcmute.edu.vn.

Partha Kayal received the Ph.D. degree in Electrical Engineering from the Indian Institute of Engineering Science and Technology Shibpur in 2016. Presently he is working as an Assistant Professor at the Department of Electrical Engineering, National Institute of Technology Silchar, India. He has published more than fifty papers in peer reviewed journals and conferences. He is an Editorial Board Member of the Scientific Reports journal. His research interests include optimization of distributed energy resources, grid integration of renewable energies, grid modernization considering energy storage and electric vehicles, reliability and power quality issues, statistical modelling and forecasting of energy, power distribution system monitoring and application of micro phasor measurement units, resiliency enabling approaches, and networked microgrid. He can be contacted at email: partha@ee.nits.ac.in.